Carrier-Phase Aided Pseudo-Noise Range Estimation at RF Frequencies

Victor A. Vilnrotter* and Kar-Ming Cheung*

ABSTRACT. — There is renewed interest in cis-lunar space exploration, including both robotic and human space missions in the near future. The current CCSDS Pseudo-noise (PN) ranging standard assumes that a terrestrial ground station defines one end of the link, achieving roughly one meter ranging accuracy under nominal conditions. However, spacecraft situational awareness and demanding docking operations require cm-level accuracy, far beyond the capabilities of current Earth-based PN-code ranging techniques. Here we develop and evaluate an ultra-precise range estimation algorithm that is capable of achieving mm level range accuracy at S-band frequencies, thus meeting future requirements for cis-lunar space exploration and situational awareness.

I. Introduction

The main idea explored in this paper is the use of carrier phase in addition to PN-code chips to estimate range. Here we describe and evaluate an algorithm for estimating range to a fraction of the carrier wavelength, which implies root-mean-square (rms) errors of millimeters at S-band frequencies.

The idea of using carrier phase in addition to PN code-phase to estimate range, operating at optical wavelengths and employing coherent optical detection, has been described and evaluated in several recent publications [1, 2, 3]. Motivated by these ideas, here we extend this concept to RF carriers suitable for near-Earth, lunar and deep-space applications. We describe range-estimation algorithms and evaluate ranging performance via MATLAB simulations supported by Cramer-Rao lower bounds on range estimator performance. The simulation model is general, but examples are specifically tailored towards S-band (~2000 MHz) or X-band (~8000 MHz) carrier frequencies, with the PN code modulated coherently onto the RF carrier such that the start of each PN chip corresponds to the rising edge of the sinusoidal carrier waveform, as practiced in the DSN for PN ranging applications.

* Communications Architectures and Research Section.

The research described in this publication was carried out by the Jet Propulsion Laboratory, California Institute of Technology, under a contract with the National Aeronautics and Space Administration.

Determining the range between two spacecraft, A and B, is initiated by spacecraft A transmitting a coherent BPSK-modulated PN code to spacecraft B, where it is transponded back to spacecraft A and processed to extract range. Alternately, the models and algorithms developed here can also be applied to radar echoes from a target of interest, however there are additional considerations in the radar problem that will not be explored here in any detail.

The received transponded signal (or radar echo) is downconverted to a convenient *IF* frequency while maintaining an integer number of *IF* cycles per chip, downsampled to the *IF* cycle and cross-correlated with the corresponding reference samples to estimate coarse range via the location of the magnitude of the complex cross-correlation peak. In addition, the phase of the cross-correlation peak is estimated and converted to range in order to refine the range estimate. Simulation results are verified via Cramer-Rao bounds on the variance of the range estimation error. It is shown that millimeter-level range estimates can be achieved, provided that sufficiently high sample-SNR can be established over the proximity link.

II. Signal Model and Ranging Concept

The modulated carrier signal is of the form $s(t) = A\cos[2\pi f_0 t + p(t)]$, where $p(t)$ is the PN-code modulation with code-length *N*, chip-rate *R*, chip-duration *T*, and correlation properties selected to meet specific cis-lunar ranging requirements. In one scenario, the modulated carrier is transmitted towards the target spacecraft from the Lunar Gateway Orbiter (LGO), arriving at the spacecraft after a one-way propagation delay of $\tau/2$ seconds. The spacecraft regenerates and re-transmits the received signal, incurring another delay of $\tau/2$ seconds thus yielding the total round-trip time-of-flight delay of τ seconds. Hence the received signal can be represented as

$$r(t) = A\cos[2\pi f_0(t-\tau) + p(t-\tau)] + n(t), \tag{1}$$

where $n(t)$ is additive zero-mean Gaussian noise representing the sum of all noise sources including background, spacecraft and receiver noise, and $p(t) = \sum_i m_i d_i p_0(t - iT)$ where $p_0(t)$ is the pulse-shape, m_i is the modulation index, and $d_i = \pm 1$. Next, the received signal-plus-noise waveform $r(t)$ is downconverted to a complex intermediate frequency $f_{IF} << f_0$ by multiplying it with a complex sinusoidal local oscillator $\tilde{s}_{LO}(t)$ at frequency $f_0 - f_{IF}$, $\tilde{s}_{LO}(t) = 2\exp[-j2\pi(f_0 - f_{IF})t]$ followed by band-pass filtering, yielding the complex signal component

$$\begin{aligned}
&\tilde{s}_{IF}(t) = 2A\cos[2\pi f_0(t-\tau) + p(t-\tau)]\exp[-j2\pi(f_0 - f_{IF})t]|_{BPF} \\
&= A\left(\exp\{j[2\pi f_0(t-\tau) + p(t-\tau)]\} + \exp\{-j[2\pi f_0(t-\tau) + p(t-\tau)]\}\right)\exp[-j2\pi(f_0 - f_{IF})t]|_{BPF} \\
&= A\exp[j2\pi f_0(t-\tau) + p(t-\tau)]\exp[-j2\pi(f_0 - f_{IF})t] \\
&= A\exp\{j[2\pi f_{IF}(t-\tau) + p(t-\tau))]\}
\end{aligned} \tag{2}$$

where we made use of the identity $\cos(x) = \frac{1}{2}[\exp(jx) + \exp(-jx)]$, and *BPF* refers to bandpass filtering. Bandpass filtering at the *IF* frequency ensures that the received signal is narrowband, hence the noise waveform can be represented as $n(t) = n_I(t)\cos(f_{IF}t) + n_Q(t)\sin(f_{IF}t)$ where $n_I(t)$ and $n_Q(t)$ are zero-mean independent in phase (*I*) and quadrature (*Q*) components, each with variance σ^2 [4].

Maximum Likelihood Estimation of Delay and Phase. Following downconversion to complex baseband via resampling, the received signal at each antenna can be modeled as an *N* dimensional vector of complex baseband time samples taken at integer multiples of the sampling interval Δt. The received samples can be represented as $\tilde{r}(i\Delta t) = \tilde{s}(i\Delta t) + \tilde{n}(i\Delta t)$. The sampling interval Δt will be assumed known in the subsequent analysis yielding the simpler representation $\tilde{r}_i = \tilde{s}_i + \tilde{n}_i$, where the variance of the complex noise samples is σ_n^2 with independent zero-mean Gaussian real and imaginary components, each with identical variance $\sigma^2 = \sigma_n^2 / 2$. A vector of *N* received samples can be represented in terms of signal and noise components as $\tilde{\mathbf{r}} = (\tilde{r}_0, \tilde{r}_1, \cdots, \tilde{r}_{N-1})$, $\tilde{\mathbf{s}} = (\tilde{s}_0, \tilde{s}_1, \cdots, \tilde{s}_{N-1})$, $\tilde{\mathbf{n}} = (\tilde{n}_0, \tilde{n}_1, \cdots, \tilde{n}_{N-1})$, and the PN modulation can be expressed as $\tilde{s}_i = A\exp\{j[p(t_i - \tau) + \theta]\}$, $t_i = i\Delta t$, where *A* is the signal amplitude. The noise variance σ_n^2 and the signal amplitude *A* are assumed to be known with the desired accuracy from previous measurements. The unknown delay τ and the unknown carrier phase θ are the remaining parameters to be estimated in this article.

For independent noise samples, the joint probability density of the complex noise vector is the product of the individual noise densities, assumed to be circular Gaussian in Equation (3):

$$p(\tilde{\mathbf{n}}) = \left(\pi\sigma_n^2\right)^{-N} \prod_{i=1}^{N} \exp(-|\tilde{n}_i|^2 / \sigma_n^2). \tag{3}$$

Given the signal parameter vector $\boldsymbol{\psi} = (\theta, \tau)$, the joint probability density of the received vector, conditioned on the phase θ and delay τ, can be expressed as:

$$p(\tilde{\mathbf{r}} \mid \boldsymbol{\psi}) = \left(\pi\sigma_n^2\right)^{-N} \prod_{i=1}^{N} \exp(-|\tilde{r}_i - \tilde{s}_i|^2 / \sigma_n^2). \tag{4}$$

The maximum likelihood (ML) estimates of the parameters are those values that simultaneously maximize the conditional joint probability density in Equation (4), or its natural logarithm known as the conditional log-likelihood function $\Lambda(\tilde{\mathbf{r}} \mid \boldsymbol{\psi})$:

$$\Lambda(\tilde{\mathbf{r}} \mid \boldsymbol{\psi}) \equiv \ln[p(\tilde{\mathbf{r}} \mid \boldsymbol{\psi})] = -N\ln(\pi\sigma_n^2) + \frac{2}{\sigma_n^2}\mathrm{Re}\left(\sum_{i=1}^{N} \tilde{r}_i \tilde{s}_i^*\right) - \frac{1}{\sigma_n^2}\sum_{i=1}^{N}|\tilde{s}_i|^2 - \frac{1}{\sigma_n^2}\sum_{i=1}^{N}|\tilde{r}_i|^2.$$

Substituting $\tilde{s}_i^* = A\exp[-j(p(t_i-\tau)+\theta)]$ for the signal samples with $|\tilde{s}_i|^2 = A^2$, we obtain

$$\Lambda(\tilde{\mathbf{r}}\,|\,\boldsymbol{\psi}) = -N\ln(\pi\sigma_n^2) + \frac{2A}{\sigma_n^2}\mathrm{Re}\left(\exp(-j\theta)\sum_{i=1}^{N}\tilde{r}_i\exp[-jp(t_i-\tau)]\right) - \frac{NA^2}{\sigma_n^2} - \frac{1}{\sigma_n^2}\sum_{i=1}^{N}|\tilde{r}_i|^2 . \quad (5)$$

Since we are only interested in estimating the phase θ and the delay τ, it follows that terms not containing these parameters cannot contribute to the maximization, hence will be ignored. Equation (5) can now be rewritten in simplified form as

$$\Lambda_0(\tilde{\mathbf{r}}\,|\,\boldsymbol{\psi}) = \mathrm{Re}\left(\exp(-j\theta)\sum_{i=1}^{N}\tilde{r}_i\exp[-jp(t_i-\tau)]\right). \quad (6)$$

First consider the estimation of the phase, θ. We recall that for any complex number $\tilde{z}$, the expression $\mathrm{Re}\{\tilde{z}\exp(-j\theta)\}$ is maximized with respect to θ when we let $\theta = \arg(\tilde{z})$, attaining its maximum value $|\tilde{z}|$. Letting $\tilde{z} = \sum_{i=1}^{N}\tilde{r}_i\exp[-jp(t_i-\tau)]$ in Equation (6) and carrying out the maximization yields the ML estimate of phase, $\hat{\theta}$, at any value of the delay τ:

$$\hat{\theta} = \arctan\left[\frac{\mathrm{Im}\left(\sum_{i=1}^{N}\tilde{r}_i\exp[-jp(t_i-\tau)]\right)}{\mathrm{Re}\left(\sum_{i=1}^{N}\tilde{r}_i\exp[-jp(t_i-\tau)]\right)}\right]. \quad (7)$$

Substituting this estimate into the simplified log-likelihood function $\Lambda_0(\tilde{\mathbf{r}}\,|\,\boldsymbol{\psi})$ maximizes it with respect to θ for any value of τ yielding $|\tilde{z}|$, hence Equation (6) can be further simplified as follows:

$$\arg\max_{\theta}\Lambda_0(\tilde{\mathbf{r}}\,|\,\boldsymbol{\psi}) = \left|\sum_{i=1}^{N}\tilde{r}_i\exp[-jp(t_i-\tau)]\right|^2 . \quad (8)$$

This last maximization can be accomplished by varying the delay τ over its uncertainty region, and selecting that value of the test delay, $\hat{\tau}$, that maximizes Equation (8). The joint estimates of carrier phase and group delay can now be expressed as

$$(\hat{\theta},\hat{\tau}) = \arg\max_{\theta,\tau}\Lambda_0(\tilde{\mathbf{r}}\,|\,\boldsymbol{\psi}) = \arg\max_{\tau}\left|\sum_{i=0}^{N-1}\tilde{r}_i\exp[-jp(t_i-\tau)]\right|^2 . \quad (9)$$

This operation is implemented by selecting a test delay τ', multiplying the *i*-th received sample $\tilde{r}_i$ by the *i*-th local sample, $\exp[-jp(t_i-\tau')]$, and evaluating the squared magnitude in Equation (9). This operation is repeated until the entire delay-uncertainty

region $(\tau_{\min}, \tau_{\max})$ known *a priori*, is covered with the desired delay-resolution, and the test-delay yielding the largest value selected as the optimal estimate of delay.

High-Resolution PN Carrier-Phase Range Estimator. The algorithm described here combines scaled versions of the delay and phase estimates to arrive at a refined estimate of range, with resolution corresponding to a small fraction of the carrier wavelength. This algorithm relies on coherent modulation of a PN sequence onto the RF carrier, which could be at S-band (2 GHz) or X-band (8 GHz), as currently employed in the DSN and also proposed for cis-lunar exploration in the near future. This coherent modulating technique is currently practiced in the DSN for PN ranging, which can achieve range resolutions of a fraction of a meter, relying entirely on the cross-correlation of the received PN code with a noiseless reference. Although coherent modulation generally implies maintaining constant phase between the start of the PN code and the start of a carrier cycle, here we set this phase to zero in order to simplify the analysis.

The phase of the return carrier signal is not affected by downconversion to an *IF* frequency, hence we are free to select an *IF* frequency that is an integer multiple of the chip-rate, yielding an integer number of *IF* cycles per chip. For example, if the carrier frequency is 2 GHz (nominal S-band frequency), and the chip-rate is 2 MCPS, then a carrier-to-*IF* downconversion factor of $\varsigma = 100$ yields 10 *IF* cycles per chip, which is known and hence can be used to rescale the measured *IF* phase to range.

With the proposed algorithm, a noiseless replica of the transmitted signal is needed to correlate with the received signal in order to extract the range. This ideal reference signal can be represented as the complex waveform $\tilde{s}_{ref}(t) = \exp\{j[2\pi f_{IF}(t) + p(t)]\}$. Here we assume that $p(t)$ is an ideal square pulse of the form $p(t) = \begin{cases} 1 & 0 < t < T \\ 0 & \text{else} \end{cases}$ in order to simplify the analysis. Incorporating the PN code model into the complex signal format yields the following expressions for the reference and return *IF* signals, respectively:

$$\tilde{s}_{ref}(t) = \exp\{j[2\pi f_{IF}(t)]\}\exp\{jp(t)\} \tag{10a}$$

$$\tilde{s}_{IF}(t) = A\exp\{j[2\pi f_{IF}(t-\tau)]\}\exp[jp(t_i-\tau)]\,. \tag{10b}$$

The *IF* frequency in Equation (10) is chosen to be such that a single cycle corresponds roughly to the delay-resolution capability of the PN code, and the reference and received waveforms are sampled at the zeros of the real part of the reference *IF* carrier (or peaks of the imaginary component). An example of such a resampled waveform is shown in Figure 1, where the modulation index was set to $m_i = \frac{\pi}{2}$, and the original high-rate primitive samples (10000 samples per chip to emulate an analog signal) was decimated by a factor of $K = 1000$, coherently with the zero-crossings of the 10 intermediate frequency cycles.

In this example, a sample-delay of 6837 samples was used for the return signals, which translates to a resampled delay of seven samples, as can be seen at the beginning of

Figure 1. Note that the in-phase and quadrature (IQ) components are constant over each chip with this re-sampling strategy, equal to the phase of the return *IF* carrier with respect to the phase of the reference *IF* signal, which is set to zero in this model. With 10000 samples per chip to simulate the analog *IF* waveform, and downsampling by a factor of $K = 1000$ yields 10 "super-samples" per chip all with the same IQ values (except for noise), as can be seen in Figure 1. Hence correlating the resampled return signal with the reference signal correctly identifies the "large-increment" delay, leaving the fine-delay to be determined via the phase of the peak of the absolute value of the return-reference cross-correlation function.

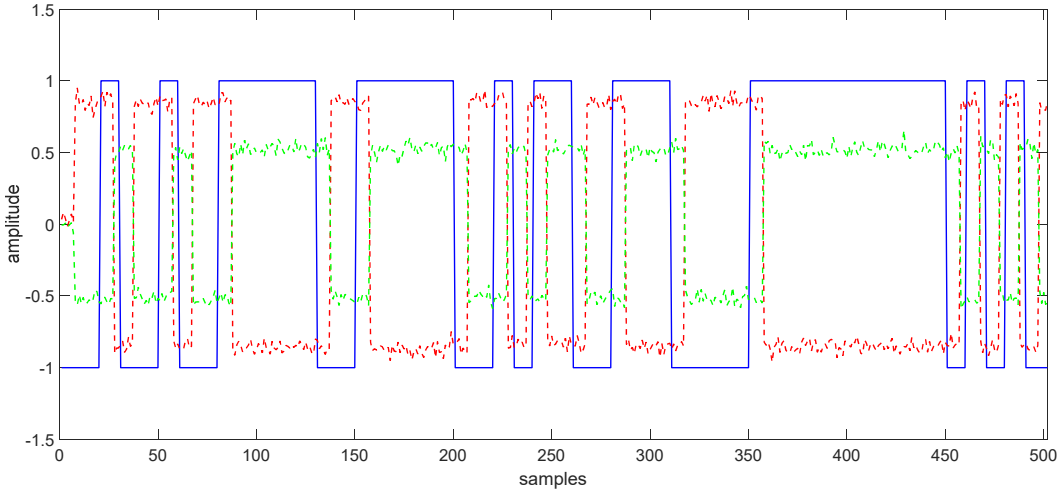

Figure 1. Coherently decimated reference (solid blue) and complex delayed return signal (real part dashed red, imaginary part dashed green), with an input delay of 6837 high-rate samples.

The phase of the correlation peak can be determined by computing the inverse tangent of the ratio of the I and Q components and converting this phase to a fractional cycle of the downconverted *IF* signal, then multiplying this result by the decimation factor in order to obtain the fractional delay in samples of the carrier. This fractional delay is then added to the large-increment delay determined from the difference of the absolute values of the reference auto-correlation and return-reference cross-correlation functions.

This algorithm basically has two distinct components: a) a large-increment component; and b) a fine-increment component. The large-increment component is estimated using the difference in the location of the peaks of the reference-signal auto- and cross-correlation functions, whereas the fine component is determined from a scaled version of the phase of the peak of the cross-correlation function.

The PN Carrier Phase algorithm consists of the following steps:

1) Determine the number of *IF* cycles per chip for the ranging application, and specify the *IF* downconversion factor ς

2) Downconvert the PN-code modulated RF carrier at frequency f_0 to an *IF* frequency of $f_{IF} = f_0 / \varsigma$, generating an integer number of cycles per chip-duration of *T* seconds

3) Sample the downconverted and PN-code modulated *IF* return signal at the zeros of the real part of the *IF* reference signal (or peaks of the imaginary part), generating decimated complex baseband samples of the *IF* return signal

4) Auto-correlate the downconverted and decimated *IF* reference signal, and determine the location of the peak of the auto-correlation function: with coherent modulation as described above, the phase of the autocorrelation peak will be zero.

5) Cross-correlate the downconverted and decimated *IF* return signal with the corresponding downconverted and decimated *IF* reference signal, and determine the location of the peak of the cross-correlation function

6) Form the difference of the locations of the peaks of the auto- and cross-correlation functions as the coarse estimate of delay

7) Determine the phase of the cross-correlation peak, and convert to cycles of the *IF* frequency to serve as the fine-estimate of delay

8) Form the sum of the rough and fine delay estimates to obtain the high-resolution estimate of delay, $\hat{\tau} = \hat{\tau}_{\text{int}} + \hat{\tau}_{\text{phase}}$, where $\hat{\tau}_{\text{int}}$ is the integer part and $\hat{\tau}_{\text{phase}}$ is the fine delay, in terms of primitive samples

9) Rescale the high-resolution delay estimate to physical range to obtain the high-resolution estimate of range.

In the following sections, we will show that range resolution on the order of centimeter accuracy can be obtained with this algorithm, with signal-to-noise ratios typical of near-Earth RF links.

III. Cramer-Rao Bounds

The variance of any unbiased estimator is lower bounded by the Cramer-Rao Bound (CRB), which can be expressed in two equivalent forms:

$$\text{a) } \operatorname{var}(\tau - \hat{\tau}) \geq \left(-E \frac{\partial^2 \Lambda(\mathbf{r} \mid \tau)}{\partial \tau^2} \right)^{-1} \quad \text{and b) } \operatorname{var}(\tau - \hat{\tau}) \geq \left(E \left\{ \left| \frac{\partial \Lambda(\mathbf{r} \mid \tau)}{\partial \tau} \right|^2 \right\} \right)^{-1}. \qquad (11)$$

For the joint phase and delay estimation problem considered here, the CRB can be determined by evaluating the components of the Fisher information matrix,

$$\mathbf{I} = \begin{bmatrix} I_{11} & I_{12} \\ I_{21} & I_{22} \end{bmatrix}, \text{where } I_{m,n} = -E\frac{\partial^2 \Lambda(\tilde{\mathbf{r}} \mid \boldsymbol{\psi})}{\partial \psi_m \, \partial \psi_n} \quad m,n = 1,2$$

and where $\psi_1 = \theta$ and $\psi_2 = \tau$, and E stands for the expectation operator. When neither parameter is known to the desired accuracy, so that joint estimation is required, the CRB for each component corresponds to the diagonal of the inverse of the Fisher Information matrix, $\mathbf{I}^{-1}$.

If one of the parameters is assumed to be known, so that only one parameter needs to be estimated, then the CRB for this single-parameter case is given by the inverse of the corresponding element of the diagonal: I_{11}^{-1} for θ, and I_{22}^{-1} for τ. In other words, the diagonal elements represent the inverse of the CRB for the given parameter, assuming the other parameter is known.

It was found via simulation that in this application, the coarse delay component is virtually error-free at the high sample-SNRs of interest, hence the incremental delay can be assumed to be known in the region of interest. This leaves the phase estimate as the dominant error source in the final computation of the delay. The CRB for the phase estimate can be found by carrying out the differentiation with respect to θ as in Equation (11a), which is the first diagonal element of the Fisher information matrix:

$$\begin{aligned} I_{11} = & -E\frac{\partial^2 \Lambda(\tilde{\mathbf{r}} \mid \boldsymbol{\psi})}{\partial \theta^2} = -E\left(\frac{2A}{\sigma_n^2}\frac{\partial}{\partial \theta}\mathrm{Re}\left(\frac{\partial}{\partial \theta}\exp(-j\theta)\sum_{i=1}^{N}\tilde{r}_i \exp[-jp(t_i-\tau)]\right)\right) \\ = & -E\left(\frac{2A}{\sigma_n^2}\frac{\partial}{\partial \theta}\mathrm{Re}\left(-j\exp(-j\theta)\sum_{i=1}^{N}\tilde{r}_i \exp[-jp(t_i-\tau)]\right)\right) \\ = & \left(\frac{2A}{\sigma_n^2}\mathrm{Re}\left(\exp(-j\theta)\sum_{i=1}^{N}E\{\tilde{r}_i \exp[-jp(t_i-\tau)]\}\right)\right). \end{aligned}$$

Substituting the received noise-corrupted samples $\tilde{r}_i = A\exp\{jp(t_i-\tau)+\theta]\} + \tilde{n}_i$, and carrying out the expectation yields

$$\begin{aligned} I_{11} = & \left(\frac{2A}{\sigma_n^2}\mathrm{Re}\left(E\sum_{i=1}^{N}\{A\exp[j(p(t_i-\tau)+\theta)]+\tilde{n}_i]\exp[-j(p(t_i-\tau)+\theta)]\}\right)\right) \\ = & \left(\frac{2A}{\sigma_n^2}\mathrm{Re}\left(\sum_{i=1}^{N}A + E(\tilde{n}_i)\right)\right) = \frac{2NA^2}{\sigma_n^2} \quad \text{since } E(\tilde{n}_i) = 0. \end{aligned}$$

If the delay is known, then the CRB for the variance of the phase estimation error is simply I_{11}^{-1}, hence the CRB on phase estimation for known delay becomes

$$\mathrm{var}(\theta - \hat{\theta}) \geq I_{11}^{-1} = \frac{\sigma_n^2}{2NA^2} = \frac{\sigma^2}{NA^2}, \tag{12}$$

where $\sigma^2 = \sigma_n^2 / 2$ is the common variance of the real and imaginary components of the complex noise sample $\tilde{n}_i$.

The received signal is effectively downconverted to complex baseband by coherent downsampling as discussed earlier, hence we evaluate the delay CRB for a complex downconverted received signal. If we set the modulation index to $m_i = \frac{\pi}{2}$, and let

$x(t-\tau) = \sum_i d_i p_0(t-\tau)$ be the real PN-code modulation, the complex signal samples can be expressed as

$\tilde{s}(t_i - \tau) = A\exp\{j[p(t_i - \tau) + \theta]\} = A\exp(j\theta)\exp\{j[\frac{\pi}{2}x(t_i - \tau)]\} = Aj\exp(j\theta)x(t_i - \tau)$.

Using the alternate form of the CRB defined in Equation (11b), we first take the derivative of the natural log of Equation (4) with respect to the delay τ, as in [5]:

$$\frac{\partial}{\partial\tau}\ln\left[\,p(\tilde{\mathbf{r}}\,|\,\boldsymbol{\psi})\right] = -\tfrac{1}{\sigma_n^2}\sum_{i=0}^{N-1}\frac{\partial}{\partial\tau}|\,\tilde{r}_i - \tilde{s}(t_i-\tau)\,|^2$$

$$= \tfrac{1}{\sigma_n^2}\sum_{i=0}^{N-1} 2\,\mathrm{Re}\left\{[\tilde{r}_i - \tilde{s}(t_i-\tau)]\frac{\partial\tilde{s}^*(t_i-\tau)}{\partial\tau}\right\} = \tfrac{1}{\sigma_n^2}\sum_{i=0}^{N-1} 2\,\mathrm{Re}\left\{\tilde{n}_i\frac{\partial\tilde{s}^*(t_i-\tau)}{\partial\tau}\right\},$$

where the last equality follows from the fact that $\tilde{r}_i - \tilde{s}(t_i - \tau) = \tilde{n}_i$. Substituting into Equation (11b), we obtain the following string of equations:

$$E\left\{\left|\frac{\partial}{\partial\tau}\ln\left[\,p(\tilde{\mathbf{r}}\,|\,\boldsymbol{\psi})\right]\right|^2\right\} = E\left\{\left|\tfrac{1}{\sigma_n^2}\sum_{i=0}^{N-1} 2\,\mathrm{Re}\left\{\tilde{n}_i\frac{\partial\tilde{s}^*(t_i-\tau)}{\partial\tau}\right\}\right|^2\right\}$$

$$= \tfrac{1}{\sigma_n^4}E\left\{\left|\sum_{i=0}^{N-1}\left\{\tilde{n}_i\frac{\partial\tilde{s}^*(t_i-\tau)}{\partial\tau} + \tilde{n}_i^*\frac{\partial\tilde{s}(t_i-\tau)}{\partial\tau}\right\}\right|^2\right\} \triangleq \tfrac{1}{\sigma_n^4}E\left\{\left|\sum_{i=0}^{N-1}\left\{\tilde{n}_i\zeta_i^* + \tilde{n}_i^*\zeta_i\right\}\right|^2\right\}$$

$$= \tfrac{1}{\sigma_n^4}\left\{\sum_{i=0}^{N-1}E\left|\tilde{n}_i\zeta_i^* + \tilde{n}_i^*\zeta_i\right|^2 + \sum_{i=0}^{N-1}\sum_{\substack{j=0\\ j\neq i}}^{N-1}E\left\{\tilde{n}_i\zeta_i^* + \tilde{n}_i^*\zeta_i\right\}\left\{\tilde{n}_j\zeta_j^* + \tilde{n}_j^*\zeta_j\right\}\right\}.$$

The double-sum is zero because disjoint noise samples are independent and hence $E(\tilde{n}_i\tilde{n}_j^*) = 0$. Furthermore, $E\left|\tilde{n}_i\zeta_i^* + \tilde{n}_i^*\zeta_i\right|^2 = 2E\,|\,\tilde{n}_i\,|^2|\,\zeta_i^*\,|^2$ because for circular Gaussian noise samples

$E(\tilde{n}_i\tilde{n}_i) = E(\tilde{n}_i^*\tilde{n}_i^*) = E(n_{I,i} + jn_{Q,i})(n_{I,i} + jn_{Q,i}) = En_{I,i}^2 + jE(n_{Q,i}n_{I,i}) + jE(n_{I,i}n_{Q,i}) - En_{Q,i}^2 = 0$

yielding the following expression:

$$E\left\{\left|\frac{\partial}{\partial\tau}\ln\left[\,p(\tilde{\mathbf{r}}\,|\,\boldsymbol{\psi})\right]\right|^2\right\}=\frac{2}{\sigma_n^4}\left\{\sum_{i=0}^{N-1}\sigma_n^2\left|\frac{\partial s^*(t_i-\tau)}{\partial\tau}\right|^2\right\}=\frac{2}{\sigma_n^2}\left\{\sum_{i=0}^{N-1}\left|-jA\exp(-j\theta)\frac{\partial x(t_i-\tau)}{\partial\tau}\right|^2\right\}$$
$$=\frac{2A^2}{\sigma_n^2}\sum_{i=0}^{N-1}\left[\frac{\partial x(t_i-\tau)}{\partial\tau}\right]^2=I_{22}. \tag{13}$$

Substituting the result of Equation (13) into Equation (11b) leads to the CRB for the error variance of any unbiased delay estimator:

$$\mathrm{var}(\tau-\tau')\geq\frac{\sigma_n^2}{2A^2}\left(\sum_{i=0}^{N-1}\left[\frac{\partial x(t_i-\tau)}{\partial\tau}\right]^2\right)^{-1}. \tag{14}$$

IV. Simulation Results

In the cis-lunar ranging application, the noise-corrupted round-trip signal received at the LGO is complex-downconverted to a suitable *IF* frequency, and compared to a local copy of the transmitted signal to extract the range. There are many plausible choices for the PN-code, however for near-Earth applications where several targets may be received simultaneously PN codes with high auto-correlation and low cross-correlation coefficients are desirable to eliminate interference. Well-known PN codes that achieve the Welch lower bound on cross-correlation are the "small Kasami" sequences, which are known to approach the Welch lower bound on cross-correlation while maintaining high auto-correlation coefficients similar to random data.

For the simulation, we selected a small Kasami sequence with period $2^8-1=255$, generator polynomial $z^8+z^4+z^3+z^2+1$ and (arbitrary) initial condition vector [0 0 0 1 1 0 0 1]. An example of this PN code is shown in Figure 2, where (0,1) has been mapped into pulses of amplitude (–1,+1) and length 10^4 high-rate samples per chip.

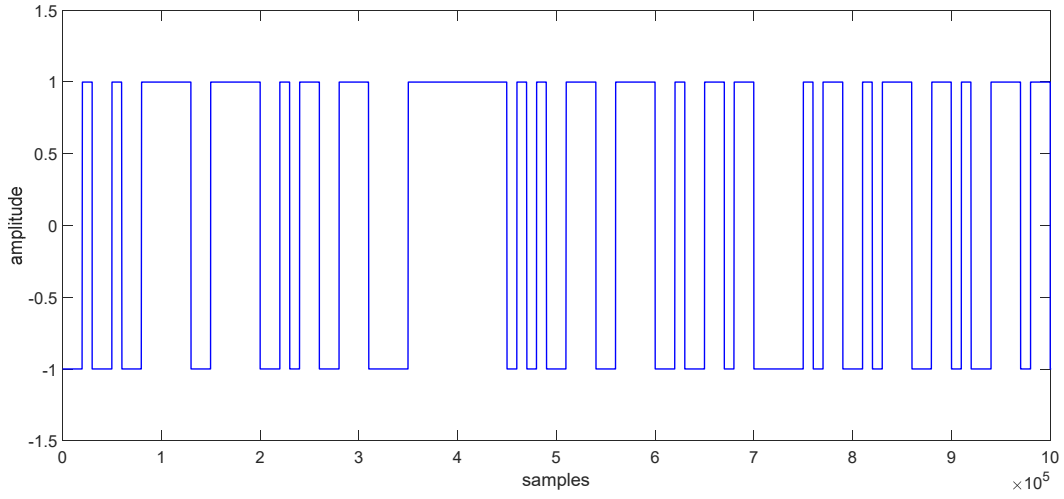

Figure 2. Example of PN-code modulation applied to the transmitted carrier, with 10000 samples per chip to approximate an analog signal.

The Kasami sequence modulation applied coherently to the carrier was downconverted to an *IF* frequency ten times greater than the chip-rate, hence there are 10 complete cycles of the complex *IF* signal per chip. An example of the imaginary parts of the local reference signal (blue) and the delayed and noise-corrupted received signal (red) is shown in Figure 3a.

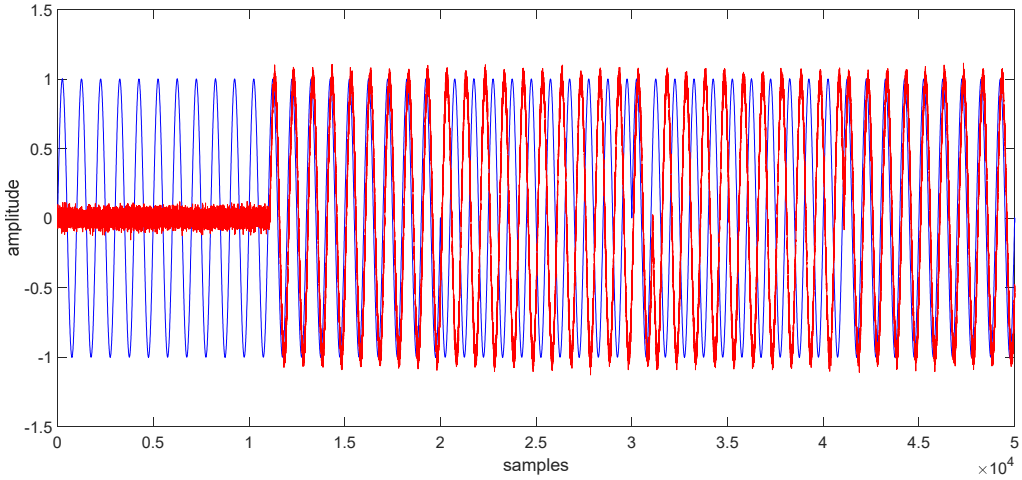

Figure 3a. Expanded view of the real parts of PN-modulated *IF* signals: local reference (blue) and return signal-plus-noise (red). A gross (integer multiples of *IF* cycle) delay or 5000 samples, and a fine delay (*IF* sub-cycle) delay of 11091 samples were applied in the simulation. Note that there are 10 *IF* cycles per chip, as can be seen in the phase-reversal of the reference (blue) signal at 20000 and 30000 samples where a single chip of 10000 samples can be seen.

In the simulation, each chip of the 255 Kasami code is sampled 10000 times, in order to simulate an analog *IF* signal and have the ability to delay the return signal by small fractions of a chip for testing purposes. A plot of the modulated *IF* signal is shown in Figure 3a, where the *IF* downconversion frequency was ten times the chip-rate, yielding 10 cycles of the return signal's in-phase and quadrature components, with 1000 samples per cycle.

The *IF*-downconverted modulated reference and return signals are sampled at the zeros of the real component (or maxima of the imaginary component) of the local reference, yielding the baseband I and Q samples shown in Figure 3b for the case of 10 cycles per chip, and hence 10 I and Q samples per chip in this example.

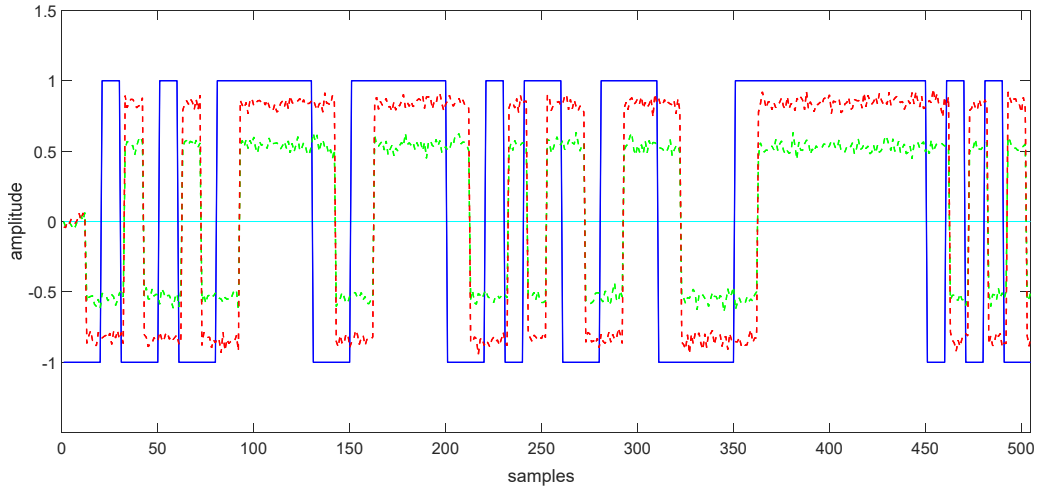

Figure 3b. Example of *IF*-downconverted and decimated local reference and return signals with a delay of 11091 samples, used to compute coarse and fine delays.

The zero-delay reference is established as the peak of the local reference auto-correlation function, shown by the solid blue plot in Figure 4. Cross-correlating the local reference with the delayed noisy return signal yields the in-phase (red dashed) and quadrature (green dashed) samples shown in Figure 4, where the absolute value of the cross-correlation peak is also shown. In this and subsequent examples 11091 samples were used, which allows the demonstration of both the coarse-delay estimate (in units of decimated samples, one sample per *IF* carrier cycle), and the fine-delay estimate obtained from the carrier phase, as the arc-tangent of the ratio of imaginary to real components.

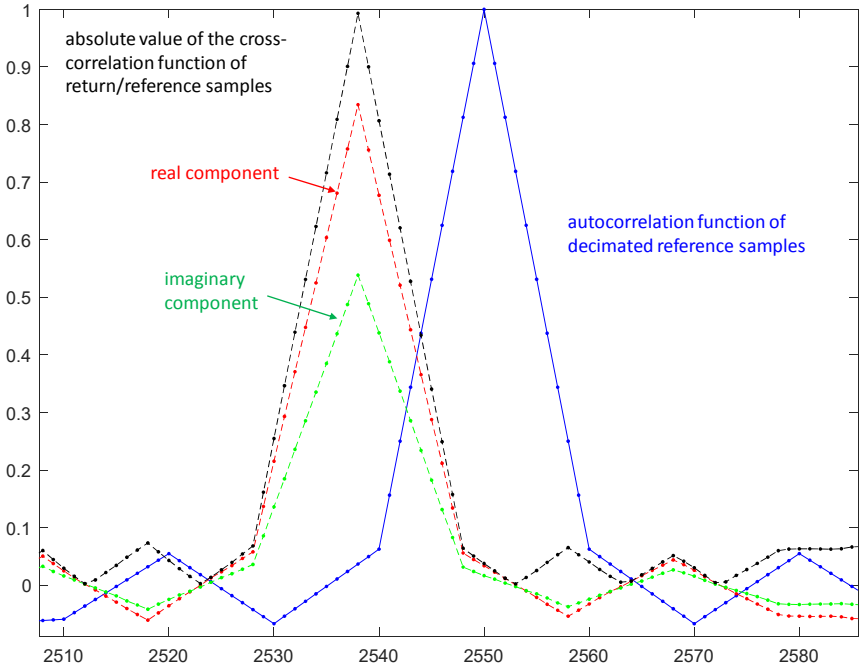

Figure 4. Example of autocorrelation and cross-correlation functions used for computing coarse delay via the difference in peak locations, and fine-delay as a scaled phase estimate obtained from the in-phase and quadrature samples at the peak of the cross-correlation function.

Having obtained the phase of the cross-correlation peak, this estimate is first converted to cycles instead of radians, then multiplied by the decimation-factor that relates primitive samples to decimated *IF* samples. Both the coarse-delay and fine-delay phase estimates are multiplied by the decimation-factor *K*, in order to relate the results to primitive samples.

The root-mean-square (rms) error of each simulation point in Figure 6 was computed from 100 delay estimates, an example of which is shown in Figure 5 for the case of 11091 sample delay applied to the return signal in the simulation, at an SNR of 17 dB. Note that the mean value of the instantaneous delay estimates is very close to the applied value, and that the observed scatter is consistent with the computed rms scatter of approximately 0.3 samples.

The total delay estimation error is shown in Figure 6, as a function of sample-SNR. The CRB for carrier-phase estimation error, scaled to represent fine-delay estimation error in terms of primitive samples is also shown as the dashed cyan line, for an input delay of 11091 primitive samples (this was selected to exercise both the integer coarse-delay and continuous fine-delay parts of the algorithm). It was found that the CRB for the coarse-delay estimation was not relevant over the sample-SNR region of interest above threshold (approximately –20 dB sample-SNR in Figure 6), because the coarse-delay samples consist of 1000 primitive samples in the simulation and such large errors do not usually occur above threshold.

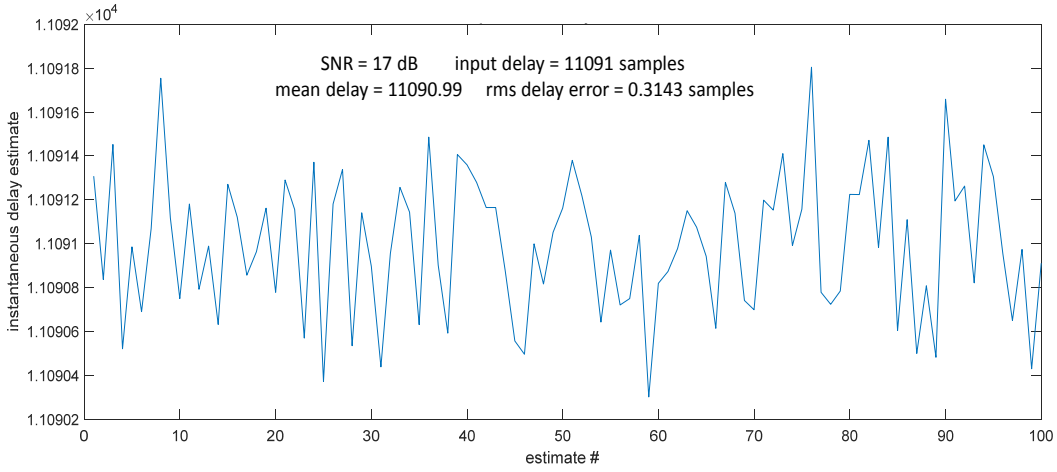

Figure 5. Example of a sequence of 100 delay estimates at a sample-SNR of 17 dB, with a simulated input delay of 11091 primitive samples, confirming the mean and rms error of the delay estimates.

To support this claim, we compute difference-function of the small Kasami sequence and form the sum of the squared differences yielding $\sum_{i=0}^{N-1}\left[\frac{\partial p(t_i-\tau)}{\partial \tau}\right]^2 = 476$, which in turn yields an rms delay error of approximately 150 primitive samples at –13 dB sample-SNR when substituted into Equation (14). This is close to the region where coarse-delay errors begin to occur in Figure 6, caused by errors in the coarse-delay estimate, and leading to catastrophic deterioration in the estimator's performance.

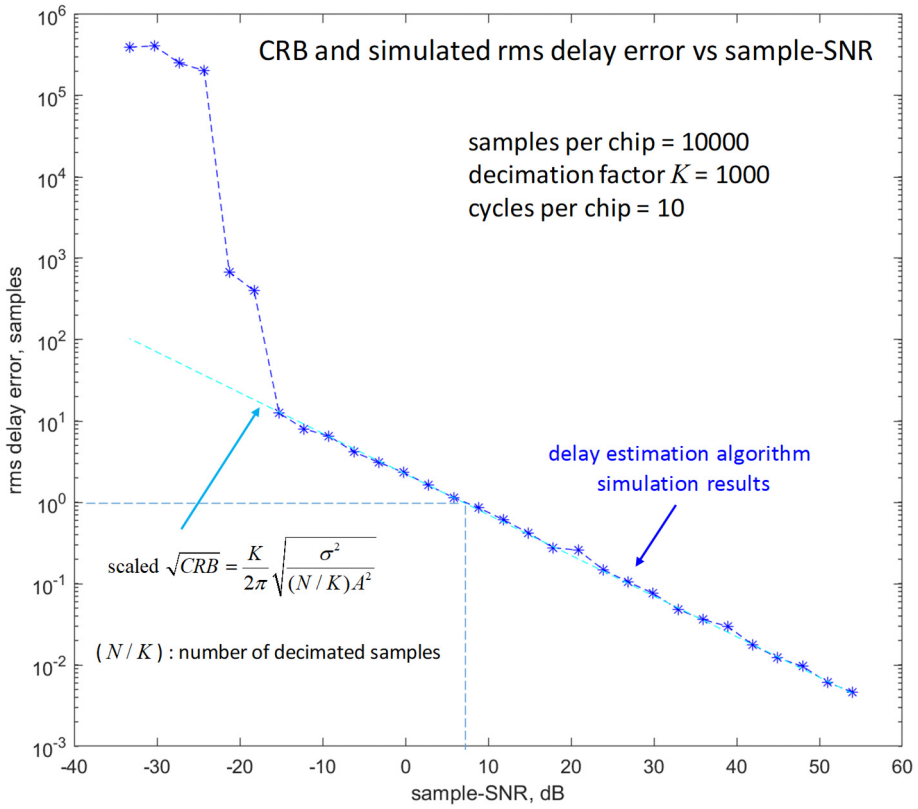

Figure 6. Scaled CRB and simulation results for the fine delay estimates, demonstrating one sample rms delay error at approximately 7 dB sample-SNR.

Example of near-Earth spacecraft ranging: Carrier frequencies of 2 GHz and 8 GHz (S-band and X-band, respectively) are currently in use in the DSN and have been proposed for future near-Earth and cis-lunar applications. For this example, consider the use of S-band carriers modulated coherently with a suitable PN code (e.g., 255 Kasami sequence) with 2 mega chips per second (MCPS) chip rate, and downconverted to 20 MHz *IF* frequency via a carrier-to-*IF* downconversion ratio of $\varsigma = 100$. This downconversion strategy yields 10 *IF* cycles per chip, sampled at 20 MSPS at the peaks of the imaginary component of the noiseless reference *IF* waveform.

Various delays were input to the simulation as integer primitive samples. With 2 MCPS chip rate, each chip delay represents roughly 150/2 = 75 meters of one-way range, therefore each primitive sample is 75/10000 = 7.5 mm of one-way range. The rms performance of the PN-phase algorithm shown in Figure 6 indicates that a sample-SNR of roughly 7 dB is required for an rms delay resolution of one primitive sample in order to achieve range-resolution on the order of a centimeter or less.

V. Conclusions

An optimal range estimation algorithm was derived and evaluated via analysis and simulation, and confirmed theoretically via Cramer-Rao lower bounds on the variance of the estimation error. A coherent PN-code modulation model was adopted, whereby the phase relation between the carrier and the PN code remained constant, as commonly practiced in DSN ranging applications. It was shown that by downconverting the carrier to a known *IF* frequency that was an integer multiple of the chip-rate and downsampled to *IF* cycles, theoretically the range information is maintained and hence accurate range measurements can be obtained with nominal sample-SNRs typical of near-Earth RF proximity links.

References

[1] G. Yang, W. Lu, M. Krainak, X. Sun, "High-precision ranging and range-rate measurements over free-space-laser communication link," In *2016 IEEE Aerospace Conference,* pp. 1–13. IEEE, 2016.

[2] G. Yang, J. Chen, K. Numata, M. Krainak, G. Heckler, C. Gramling, "Optical carriers phase based high-precision ranging and range rate measurements in coherent optical communication." In *2018 IEEE Aerospace Conference,* pp. 1–10. IEEE, 2018.

[3] V. Vilnrotter and J. Breidenthal, "Maximum likelihood estimation of delay and phase for chirped signals," *The Interplanetary Progress Report,* vol. 42-215, Jet Propulsion Laboratory, Pasadena, California, pp. 1-15, November 15, 2018. https://ipnpr.jpl.nasa.gov/progress_report/42-215/42-215B.pdf

[4] S. O. Rice, "Mathematical analysis of random noise," *Bell Syst. Tech. J.,* vol. 23, pp. 282–332, July 1944.

[5] R. A. Iltis, "Joint Estimation of PN Code Delay and Multipath Using the Extended Kalman Filter," *IEEE Transactions on Communications,* vol. 38, no. 10, 1990.